

Significant Contribution to Strength Enhancement from Deformation Twins in Thermomechanically Processed $\text{Al}_{0.1}\text{CoCrFeNi}$ Microstructures

Sindhura Gangireddy, Daniel Whitaker, and Rajiv S. Mishra

(Submitted September 4, 2018; in revised form January 8, 2019; published online January 31, 2019)

Strengthening mechanisms from thermomechanical processing treatments were explored in single-phase FCC high-entropy alloy $\text{Al}_{0.1}\text{CoCrFeNi}$. Cold work offers substantial strengthening in this low stacking fault energy material owing to the resultant high work hardening rates. An enormous increase in yield strength of $\sim 275\%$ was obtained in 40% rolled material, but was accompanied by a steep drop in ductility. Recovery and recrystallization annealing treatments were investigated for improving elongation and obtaining better balance of strength–ductility combinations. Formation of novel microstructures from the different processing routes was examined. X-ray diffraction peak broadening and mechanical test results were coupled to estimate micro-strain in the different conditions and understand micro-strain's correlation to strength. Retention of large-scale deformation twins formed during cold rolling is shown to play a key role in elevation of yield strength after heat treatments.

Keywords $\text{Al}_{0.1}\text{CoCrFeNi}$, dislocation hardening, high-entropy alloy, mechanical properties, partial recrystallization, recovery, thermomechanical processing

1. Introduction

High-entropy alloys (HEAs) mark emergence of a new paradigm of metallic alloy development of stabilizing simple microstructures with multiple principal elements in equimolar proportions. Significant multi-element effects were proposed in HEAs, e.g., high entropy, sluggish diffusion, lattice distortion and cocktail effects, and have been extensively studied (Ref 1–4). Their potential for solid solution strengthening combined with good ductility, if the solid solution phase possesses a simple crystal structure, makes them appealing candidates for structural applications. $\text{Al}_x\text{CoCrFeNi}$ is a prominent alloy system identified on the basis of this design strategy of simple crystal structures. It changes from FCC to BCC structure with increasing aluminum content and displays a wide spectrum of mechanical behavior (Ref 5–8). At low Al contents, such as $\text{Al}_{0.1}\text{CoCrFeNi}$ ($x = 0.1$), the HEA is of single-phase FCC crystal structure. Its cast form is composed of large grains and has a low YS of 150–200 MPa. Some recent studies (Ref 9) have investigated Hall–Petch effect in this HEA, but other strengthening mechanisms have not yet been fully explored. Due to the stability of the FCC phase even at higher temperatures in this low-Al HEA, precipitation strengthening is not possible. But cold work-based strengthening is very promising because of its low stacking fault energy (SFE), estimated to be less than 30 mJ/mm^2 (Ref 10). Dissociation of

several dislocations into $1/6 \langle 112 \rangle$ Shockley partials has been reported in another single-phase FCC HEA FCC CoCrFeNiMn (Ref 11) with low SFE. Such wide separation between partials can inhibit cross-slip and suppress dynamic recovery. So lower SFE generally translates to higher work hardening rates. Gali and George (Ref 12) have conducted a study on the tensile properties of thermomechanically processed CoCrFeNiMn, but the room-temperature YS remained below 300 MPa in all their processed conditions. But $\text{Al}_{0.1}\text{CoCrFeNi}$ has a lower SFE and so offers greater potential for substantial strength gain from cold working.

In this study, we conducted a detailed investigation on strength enhancement in $\text{Al}_{0.1}\text{CoCrFeNi}$ by thermomechanical processing. The cast material was subjected to a combination of different annealing treatments following cold work. Microstructural and mechanical test results from these processed conditions are compared to the cast and pure rolled conditions to demonstrate their notable strength improvements while retaining sufficient ductility for engineering applications.

2. Experimental Procedure

$\text{Al}_{0.1}\text{CoCrFeNi}$ was obtained from a commercial vendor, Smart Materials Inc., and 20-mm-thick plates of the cast ingot were sectioned. These plates were unidirectionally rolled at room temperature to thickness reductions of 20 and 40%. These rolled plates were then subjected to annealing treatments, two of which were in recovery temperature range ($550^\circ\text{C}/24 \text{ h}$, $620^\circ\text{C}/50 \text{ h}$), and two at higher temperatures in recrystallization regime ($700^\circ\text{C}/5 \text{ h}$, $800^\circ\text{C}/1 \text{ h}$). The plates were placed inside preheated furnaces and then cooled by water quenching after specified hold time, in order to eliminate microstructural evolution during heating and cooling ramps. The microstructures of these various heat-treated conditions were studied using scanning electron microscope (SEM) and electron backscatter diffraction (EBSD). X-ray diffraction (XRD) was used to study

Sindhura Gangireddy, Daniel Whitaker, and Rajiv S. Mishra, AMMPI, University of North Texas, Denton, TX 76207. Contact e-mail: sindhu.g.reddy@gmail.com

the phases and peak broadening from cold work. Tensile test specimens of 10 mm gauge length, 2 mm width and 0.5 mm thickness were then EDM cut from the cast, pure rolled and heat-treated plates. In the latter conditions, the sample gauge length was aligned perpendicular to the rolling direction. The samples were subjected to tensile loading at 10^{-3} s⁻¹ strain rate to obtain their quasi-static mechanical properties.

3. Results and Discussion

The contrast in the microstructures and the mechanical properties of cast versus rolled conditions is highlighted in Fig. 1. The SEM image of the cast material in Fig. 1(a) shows a microstructure composed of large equiaxed grains, while the EBSD of 40% rolled material in Fig. 1(b) shows elongated grains with large-scale deformation twins, > 100 μm in length. It is well known that FCC alloys with low stacking fault energy (SFE) can deform by twinning even at low strain rates (Ref 13, 14). Al_{0.1}CoCrFeNi high-entropy alloy is estimated to have a very low SFE of 30 mJ/mm² (Ref 10), so deformation twinning is naturally anticipated during the sub-dynamic process of cold milling. The presence of deformation twins in the cold rolled condition is clearly marked by a spike in the number fraction of Σ3 boundaries with 60° misorientation, representing twin fault planes, as seen from inset box in Fig. 1(b).

The XRD patterns revealed all cast and rolled conditions to be single-phase FCC (Fig. 1c). With increasing cold work the peaks are observed to get broader, indicating higher dislocation storage. Micro-strain in these microstructures can be derived

using Williamson–Hall method (Ref 15, 16), a classical technique for obtaining quantitative information of anisotropy in broadening (Ref 17, 18).

$$\beta \cos \theta = \frac{K\lambda}{D} + 4\varepsilon \sin \theta \quad (\text{Eq 1})$$

where β is the broadening/full width at half maximum (FWHM) of the peak, θ is the angle of diffraction of the peak, K is a constant, λ is the wavelength of x-rays, D is the crystallite size (here ~ 500 μm), and ε is the micro-strain. So the slope of the linear fit of $\beta \cos \theta - 4 \sin \theta$ plot of two or more peaks can be used to estimate micro-strain in a given condition. Figure 1(d) plots $\beta \cos \theta - 4 \sin \theta$ using the three XRD peaks (111), (200) and (220) in each of cast, 20% rolled (20CR) and 40% rolled (40CR) conditions. In Fig. 1(d), the slope of the as-cast condition is quite small, which is anticipated (Ref 16) because here lattice would be relatively relaxed. But upon cold work micro-strain increased rapidly in 20CR ($\varepsilon = 0.054$) and 40CR ($\varepsilon = 0.161$) conditions. Figure 1(e) plots this increase in micro-strain with % cold work done on the material. The micro-strain in the crystal structure is directly related to its stored dislocation density, ρ (Ref 16):

$$\rho = \frac{2\sqrt{3}}{Db} \quad (\text{Eq 2})$$

where b is Burgers vector, in FCC structure, $b = \sqrt{2}\frac{a}{2}$. Slope ($\frac{\lambda}{2a}$) of $\sqrt{(h^2 + k^2 + l^2)} - \sin \theta$ plot in Fig. 1(f) was used in deriving lattice parameter $a = 0.358$ nm, identical to previous reports (Ref 19). So the Burgers vector in this lattice is $b = 0.255$ nm.

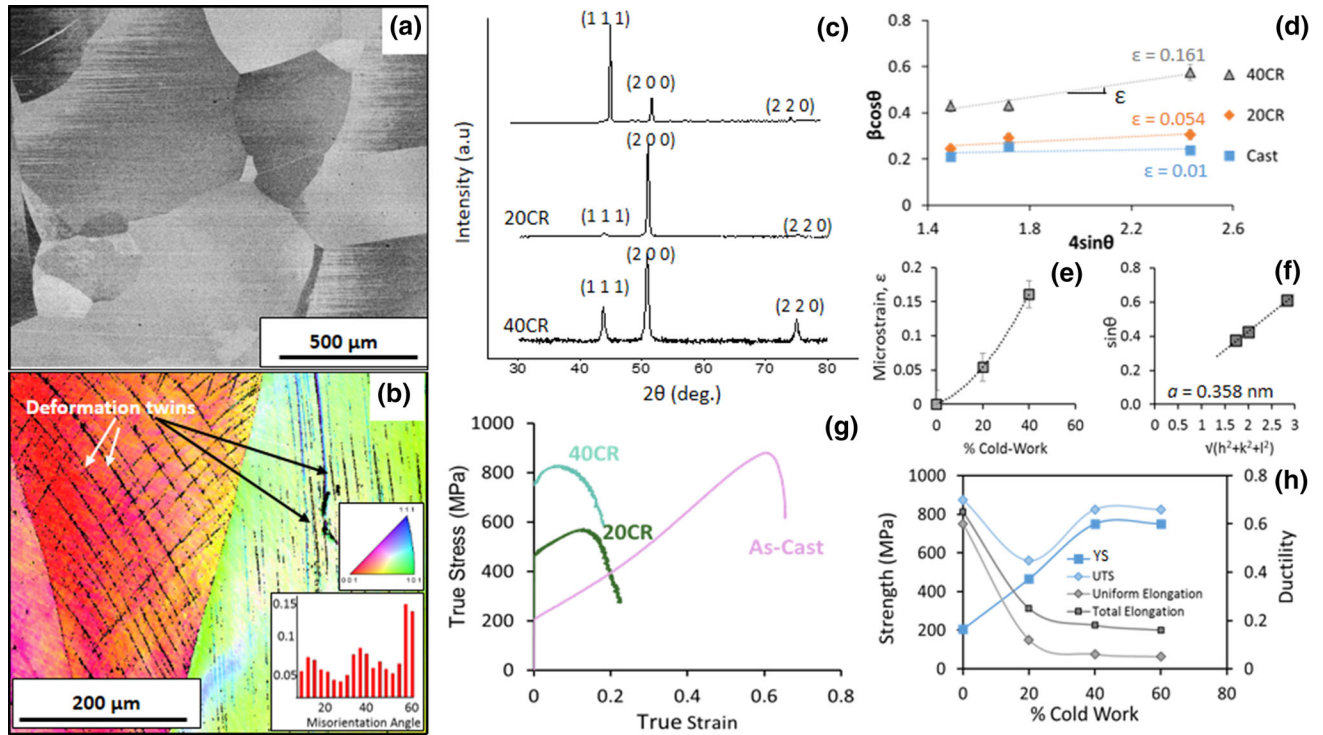


Fig. 1 Microstructure and mechanical properties of the as-cast and rolled conditions: (a) SEM image of the cast material, (b) EBSD of 40% rolled condition (40CR), (c) XRD patterns showing FCC peaks, (d) the use of peak broadening for derivation of micro-strain from slope of linear fit of $\beta \cos \theta - 4 \sin \theta$ plot, (e) increase in micro-strain with % cold work, (f) calculation of lattice parameter, a , (g) true stress–true strain curves from quasi-static tensile testing and (h) variation of the mechanical properties with the extent of cold work

An important observation from these estimates is that dislocation storage capability is very high in this HEA composition owing to its low SFE (Ref 14). At a mere 40% cold work, the micro-strain reached 0.161. Low SFE results in wide spacing between dislocation partials, inhibiting cross-slip and hence dynamic recovery processes. As a result, higher dislocation densities, translating to higher micro-strain, are obtained even at relatively lower strain levels (Ref 20).

The stress-strain curves from mechanical testing of these cast and rolled conditions are shown in Fig. 1(g). Critical properties such as YS, UTS, uniform elongation and total elongation are summarized in Fig. 1(h). The as-cast material showed a low YS of about 200 MPa and a ductility of over 60%, comparable to the values reported in the literature (Ref 9, 21, 22). It demonstrated very strong work hardening, which prevented early onset of necking instability, and a substantial UTS of over 875 MPa was attained. Upon cold rolling to 20%, yield strength improved \sim 465 MPa in 20CR. But this rolled condition had lower ductility of only 12% uniform elongation, and this directly affected UTS which was merely 560 MPa. With cold rolling up to 40%, strength continued to improve to reach a high YS = 750 MPa in 40CR and ductility dropped further to 6% uniform elongation. However, due to the higher YS, UTS recovered back to 825 MPa in 40CR.

As shown in Fig. 1(g), the increase in YS with cold work appeared linear up to 40%, but most of the loss in ductility occurred by 20%, so it showed a drop in UTS. But UTS was recuperated at 40% due to higher YS. Hence, the 40% cold-worked material was chosen as the ideal candidate for further annealing treatments. Two of the heat treatments were performed at low temperatures to facilitate recovery of the stored cold work. The first annealing treatment was at 550 °C with a hold time of 24 h, while the second treatment was chosen at a higher temperature of 620 °C with longer duration of 50 h. The microstructures, XRD data and mechanical properties of these recovered conditions are presented in Fig. 2.

The microstructures after low-temperature annealing at 550 °C/24 h and 620 °C/50 h, shown in Fig. 2(a) and (b), showed several signs of remnant cold work. The microstructures had contrast variations within grains in the shape of bands. We termed these bands “deformation bands” and speculated that they formed when one portion of the grain underwent more strain and rotated the grain slightly, without actually forming a grain boundary. Many of the large-scale deformation twins from rolling (see Fig. 1b) vanished, but some were nevertheless detected in the 550 °C/24 h condition from misorientation line profiling, as highlighted by Line 1 scan. Inset in Fig. 2(a) shows the 60° misorientation from a twin fault plane in 550 °C/24 h condition. After heat treatment at further elevated temperatures, these large deformation twins appear to be completely recovered and were not detected in the 620 °C/50 h condition. The XRD diffraction patterns in Fig. 2(c) confirm the two recovery annealed conditions to be still single-phase FCC. The peak broadening shows a slight reduction indicating some recovery in micro-strain. Figure 2(d) illustrates the effect of the two recovery annealing treatments on 40CR’s micro-strain. Micro-strain dropped to 0.139 after 550 °C/24 h treatment and to 0.117 after 620 °C/50 h annealing. The mechanical properties of the recovered conditions shown in Fig. 2(f), however, demonstrate an ominous drop in strength after annealing. Both recovery treatments significantly improved ductility, bringing the total elongation to \sim 40%. But as the treatment temperature increased, the strength gains from

cold rolling were sacrificed to a higher extent. The 550 °C/24 h treatment showed a lower YS of 562 MPa as compared to 40CR with 750 MPa YS, while 620 °C/50 h condition had further lower YS = 414 MPa.

The total yield strength of a microstructural condition is generally given by a summation of internal stresses, dislocation hardening and grain boundary strengthening:

$$\sigma = \sigma_o + M\alpha Gb\sqrt{\rho} + \frac{\beta}{\sqrt{D}} \quad (\text{Eq 3})$$

From Eq 2, replacing dislocation density with micro-strain:

$$\sigma = \sigma_o + M\alpha Gb\sqrt{\frac{2\sqrt{3}}{Db}\sqrt{\varepsilon}} + \frac{\beta}{\sqrt{D}} \quad (\text{Eq 4})$$

where the first term accounts for internal stresses (both lattice friction and solid solution strength contributions), the second term accounts for the Taylor contribution in Bailey–Hirsch relationship (Ref 23), and the third term arises from Hall–Petch relationship. In the second term, M is average Taylor factor, α is a constant, and G is the shear modulus. This term describes the strength gain from micro-strain/dislocation hardening.

But in the case of Al_{0.1}CoCrFeNi HEA which has twinned extensively during cold rolling, there would be additional strength contribution from deformation twins. Figure 2(e) plots yield strengths of cast, rolled and recovery annealed conditions with square roots of their measured micro-strains. From Eq 4, YS was expected to linearly increase with micro-strain, but Fig. 2(e) shows a clear deviation in several of the conditions which had deformation twins. The cast and the 620 °C/50 h conditions were the only conditions that were largely free of deformation twins. So the slope of the dotted black line connecting these two points, 625 MPa, would be α' , a constant comprising of all the factors in Bailey–Hirsch formula = $M\alpha Gb\sqrt{\frac{2\sqrt{3}}{Db}}$. This linear line represents the predicted contribution from pure dislocation hardening at different micro-strain levels. The deviations seen in the cold rolled (20CR, 40CR) and the 550 °C/24 h conditions must therefore originate from the presence of deformation twins in these microstructures. These twin strength contributions, highlighted as red dotted lines, cause the total YS of 20CR, 40CR and 550 °C/24 h condition to elevate above the predicted level. Twin strength contributions can be seen to rise with the extent of cold work, because rolling process is the origin of deformation twinning and further cold work would introduce more twin boundaries into the material. So 40CR naturally had much higher twinning contribution than 20CR. But after annealing at 550 °C/24 h, there was significant recovery of deformation twins, as seen from a comparison of Fig. 1(b) and 2(a), and twinning contribution in 550 °C/24 h drops.

The other two treatments were in recrystallization regime, 700 °C/5 h and 800 °C/1 h, and generated very curious microstructures due to partial recrystallization. The microstructures, XRD patterns and mechanical properties of these conditions are summarized in Fig. 3 and 4. Both conditions showed heterogeneous structures composed of regions with large prior elongated grains and regions with smaller recrystallized grains. But there were several disparities between the two microstructures. The low-magnification SEM images show that the recrystallized regions were more dispersed in the

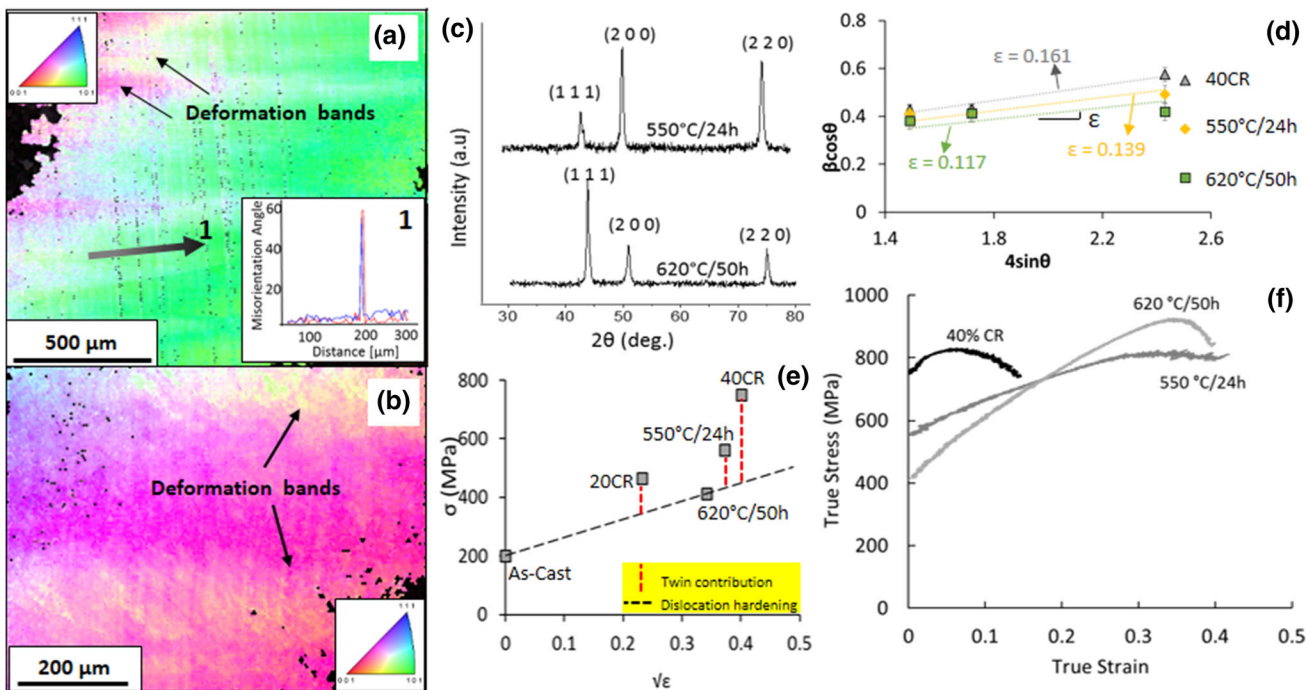


Fig. 2 Microstructure and mechanical properties after low-temperature annealing, 550 °C/24 h and 620 °C/50 h conditions. (a) EBSD of 550 °C/24 h with inset of misorientation profiling along Line 1, (b) EBSD of 620 °C/50 h. Both show remnant cold work signs as intragranular contrast in band form. (c) XRD patterns showing FCC peaks, (d) derivation of micro-strain from peak broadening showed small reduction in micro-strain after recovery annealing, (e) $\sigma - \sqrt{\varepsilon}$ plot showing elevated strength in some conditions than prediction from dislocation hardening; this difference was attributed to strength contribution from deformation twins, and (f) stress-strain curves of the pure rolled and recovered conditions

700 °C/5 h condition (Fig. 3a), and within a prior grain, there were some recrystallized areas and some remnant areas. In the 800 °C/1 h condition, the recrystallized regions appeared tightly packed (Fig. 3c). Each prior grain here was either fully recrystallized or completely untransformed. The EBSD images showed that the recrystallized grains in 700 °C/5 h had contrast variation within grains indicating intragranular cold work storage (Fig. 3b). This was eliminated after 800 °C/1 h whose recrystallized grains were fully equiaxed (Fig. 3d). The size of the 800 °C/1 h recrystallized grains was also larger at ~ 50 μm (Fig. 3d, inset), whereas the 700 °C/5 h recrystallized grains were ~ 8 μm in diameter (Fig. 3b, inset). This suggested that grain growth also occurred during 800 °C. Together, these differences inferred that during 700 °C/5 h the formation of new grain boundaries occurred by dislocation rearrangement and annihilation, whereas nucleation and grain boundary sweep occurred at 800 °C/1 h. So 800 °C/1 h is a true partial recrystallization treatment for this Al_{0.1}CoCrFeNi alloy, sufficient to cause full recrystallization, provided the prior grain had adequate strain energy. Wu et al. (Ref 21) observed full recrystallization in 60% cold rolled Al_{0.1}CoCrFeNi HEA with the same 800 °C/1 h annealing conditions. In our material with 40% cold work, there must have been strain inhomogeneity at the grain level as a result of which not all grains had enough strain to trigger recrystallization, leading to an overall partially recrystallized microstructure. The XRD diffraction patterns show that even after high-temperature annealing, the HEA remained in FCC crystal structure.

Understanding the strength-microstructure correlations is more complicated in these heterogeneous microstructures. The YS of a generic partially recrystallized structure, with fraction of recrystallization X , can be estimated as:

$$\begin{aligned} \sigma_{\text{partial reXn}} = & \sigma_0 + X \frac{\beta}{\sqrt{d}} + (1-X) \frac{\beta}{\sqrt{D}} + (1-X)(\alpha' \sqrt{\varepsilon}) \\ & + \sigma_{\text{TW}} \end{aligned} \quad (\text{Eq } 5)$$

where β is the Hall-Petch constant, d is the recrystallized grain size, D is the original prior grain size, and ε_r is the remnant micro-strain in these prior grains after any recovery of cold work at the high temperatures. σ_{TW} is any additional strength contribution from any unrecovered deformation twins in the unrecrystallized regions. Given that the cast material's strength is given from Eq 3 as:

$$\sigma_{\text{cast}} = \sigma_0 + \frac{\beta}{\sqrt{D}}$$

The strength difference between a partially recrystallized structure and cast condition will be:

$$\sigma_{\text{partial reXn}} - \sigma_{\text{cast}} = X \beta \left[\frac{1}{\sqrt{d}} - \frac{1}{\sqrt{D}} \right] + (1-X)(\alpha' \sqrt{\varepsilon}) + \sigma_{\text{TW}} \quad (\text{Eq } 6)$$

The first term on RHS reflects the Hall-Petch strength addition from grain refinement in the recrystallized regions. Smaller grains have a higher volume fraction of grain boundaries which could impede dislocation motion. The second term represents the Taylor contribution from remnant cold work in the prior grains, while the third term is a possibility of strength addition from deformation twin presence. So, together, the second and third terms represent overall strength gain from

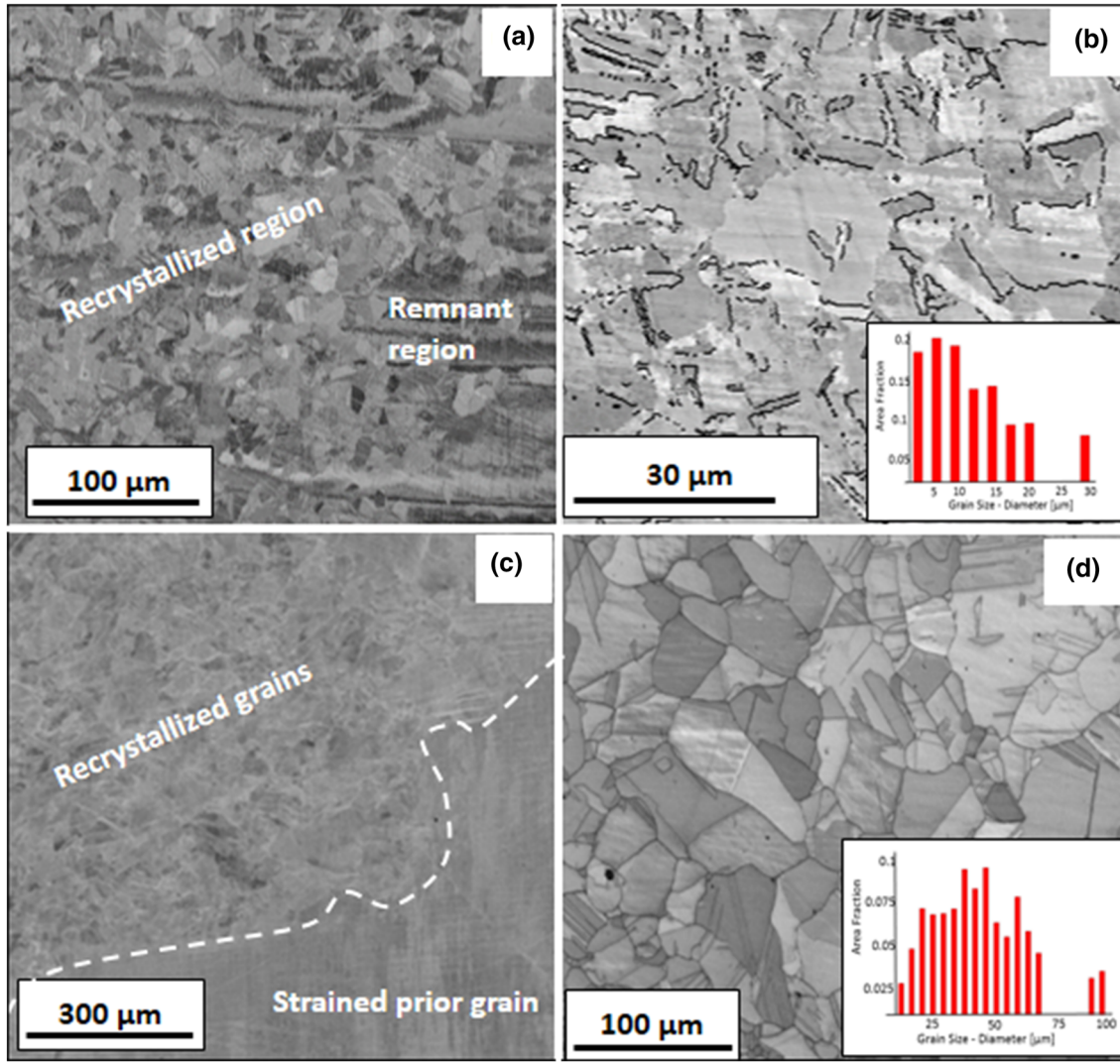


Fig. 3 Microstructures after high-temperature annealing: (a) SEM image of 700 °C/5 h, (b) EBSD image of 700 °C/5 h, (c) SEM image of 800 °C/1 h and (d) EBSD image of 800 °C/1 h

remnant cold work, originating from unrecovered micro-strain as well as deformation twins.

$$\begin{aligned} \sigma_{\text{partial reXn}} - \sigma_{\text{cast}} - X\beta\left[\frac{1}{\sqrt{d}} - \frac{1}{\sqrt{D}}\right] &= (1-X)(\alpha'\sqrt{\varepsilon}) + \sigma_{\text{TW}} \\ \sigma_{\text{CR,r}} &= \alpha'(1-X)\sqrt{\varepsilon} + \sigma_{\text{TW}} \end{aligned} \quad (\text{Eq } 7)$$

The mechanical response in Fig. 4(a) shows that the 700 °C/5 h treatment which resulted in smaller, reorganized grains showed a YS of 505 MPa, whereas the 800 °C/1 h treatment with larger, equiaxed and recrystallized grains showed a lower YS of 377 MPa.

From a collage of low-magnification SEM images, one of which is shown in Fig. 4(c), the fraction of recrystallized regions in 800 °C/1 h was calculated to be ~ 0.35 . EBSD (Fig. 4d) showed the recrystallized grain size to be $\sim 50 \mu\text{m}$, while the prior grains were about $500 \mu\text{m}$. Komarasamy et al. (Ref 9) calculated the Hall-Petch constant (β) of this HEA to be $371 \text{ MPa } \mu\text{m}^{0.5}$. So the first term in Equation 6 = $0.35 * 371 \left[\frac{1}{\sqrt{50}} - \frac{1}{\sqrt{500}} \right] \text{ MPa} = 13 \text{ MPa}$. However, the total yield

strength difference is 177 MPa. So the remnant cold work strength ($\sigma_{\text{CR,r}}$) was 164 MPa.

The fraction of recrystallized regions in 700 °C/5 h is estimated to be 0.42, and as the recrystallized grain size was much smaller, $8 \mu\text{m}$, the Hall-Petch strength addition was much larger: $X\beta\left[\frac{1}{\sqrt{d}} - \frac{1}{\sqrt{D}}\right] \sim 55 \text{ MPa}$. The difference in the YS of 700 °C/5 h (505 MPa) and cast (200 MPa) conditions was 305 MPa, so the remainder of the YS gain was attributed to the remnant cold work, $\sigma_{\text{CR,r}} = 250 \text{ MPa}$.

Figure 4(d) plots these remnant cold work strength contributions ($\sigma_{\text{CR,r}}$) with respect to $(1-X)\sqrt{\varepsilon}$ in the two recrystallized conditions along with a limiting case of zero remnant strain which leads to zero Taylor contribution. The linear dotted line represents the Taylor contributions, and its slope is set from the earlier calculation of $\alpha' = 625 \text{ MPa}$. Once again, there was a perceptible deviation in both the recrystallized conditions which showed higher YS. The deviation was more pronounced in 700 °C/5 h, indicating it retained a higher density of remnant deformation twins along with a higher micro-strain level. This is in compliance with our earlier hypothesis that the new grain boundaries in 700 °C/5 h were formed from dislocation

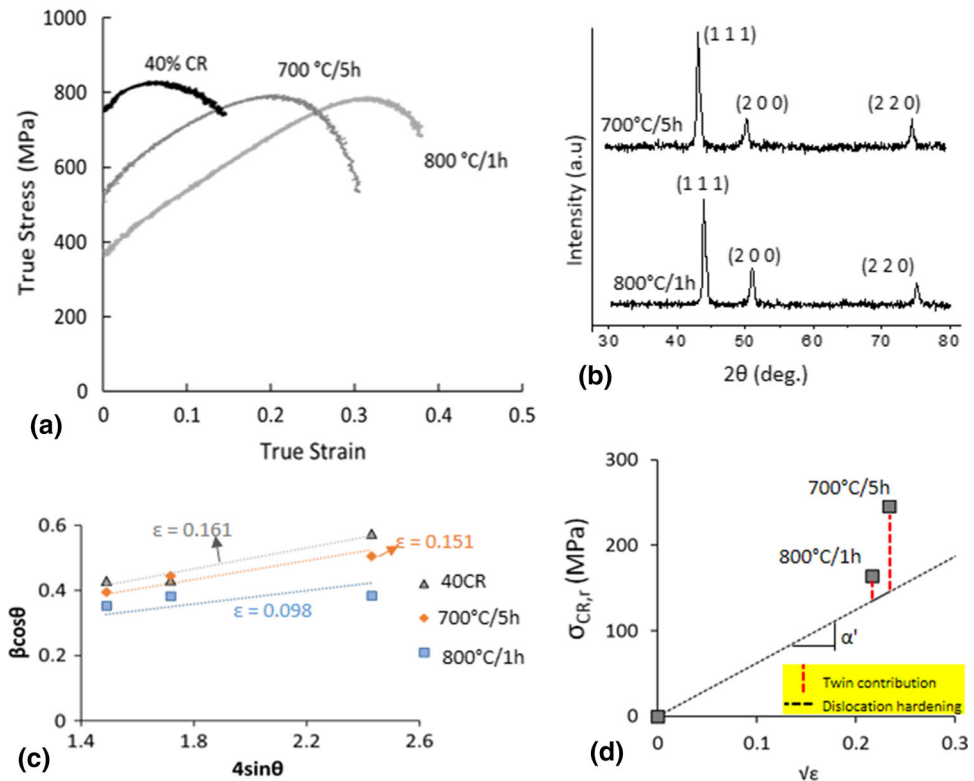


Fig. 4 Mechanical response and XRD data after high-temperature annealing at 700 °C/5 h and 800 °C/1 h. (a) Stress–strain curves of partially recrystallized conditions, (b) XRD patterns showing FCC crystal structure, (c) peak broadening used in derivation of micro-strain from slope of linear fit of $\beta \cos\theta$ – $4\sin\theta$ plot and (d) strengthening from remnant cold work plotted as a function of square root of remnant micro-strain showing elevated strength than Taylor contribution predictions

rearrangement rather than nucleation. The recovery of both dislocations/micro-strain and deformation twins is higher at further elevated temperatures, so 800 °C/1 h condition showed a lower micro-strain level along with small twin contribution to strength. This was also reflected in the mechanical response showing lower strength but higher ductility. So the remnant deformation twins in the unrecrystallized regions are associated with higher strength.

In the several different types of microstructures investigated in this study: pure rolled, low-temperature recovery annealed and high-temperature partially recrystallized conditions, deformation twinning played a key role in elevating the strength of this alloy beyond the opportunity from pure dislocation hardening.

4. Conclusion

Single-phase FCC HEA A_{0.1}CoCreFeNi of reported extremely low stacking fault energy was thermomechanically processed. Cold rolling followed by annealing generated vastly different microstructures and mechanical properties. XRD measurements were used to estimate the micro-strain, which were then correlated to the observed tensile yield strengths. The main observations from this study are summarized below:

- Cold work was found to be a very strong strengthening mechanism in single-phase FCC HEA A_{0.1}CoCreFeNi due

to its low SFE. Extensive deformation twinning was observed in the rolled microstructures. While the cast material showed a low YS of 200 MPa, 20% cold work resulted in YS of 465 MPa and 40% cold work increased YS further to 750 MPa.

- Low-temperature annealing, 550 °C/24 h and 620 °C/50 h, resulted in progressive recovery of cold work and relaxation of micro-strain. 550 °C/24 h had a small density of unrecovered deformation twins that were not detected in 620 °C/50 h. The 550 °C/24 h recovered material showed YS of 562 MPa, while 620 °C/50 h showed further lower 414 MPa.
- High-temperature annealing created heterogeneous microstructures from partial recrystallization. 700 °C/5 h formed new grain boundaries from dislocation rearrangement and had dispersed, 8-μm-sized grains, while 800 °C/1 h resulted in nucleation of fully equiaxed recrystallized grains, coarse from grain growth ~ 50 μm. However, recrystallization occurred only in some prior grains that fully transformed. The recrystallized prior grains had much higher micro-strains after 700 °C/5 h which had YS of 505 MPa than the YS of 377 MPa of 800 °C/1 h, indicating higher recovery at elevated temperatures. The overall combination of higher micro-strain, more remnant deformation twins and smaller recrystallized grain resulted in 700 °C/5 h condition having a higher YS of 505 MPa than 800 °C/1 h condition with only 377 MPa YS.
- The presence of deformation twins was associated with a spike in yield strength of the condition, beyond the pre-

- dicted Taylor contributions from dislocation hardening.
- The heat-treated conditions offered much higher strength than the cast condition while retaining a good level of ductility.

Acknowledgments

The work was performed under a cooperative agreement between the Army Research Laboratory and the University of North Texas (W911NF-16-2-0189). We also acknowledge the Materials Research Facility at UNT for microscopy facilities.

Data Availability

The raw data and the processing required to reproduce these findings are available to download and will be uploaded along with the manuscript.

References

1. M.C. Gao, *High-Entropy Alloys*, Springer, New York, 2016
2. J.W. Yeh, Novel Alloy Concept, Challenges and Opportunities of High-Entropy Alloys, *Frontiers Design Materials*, B. Raj, Ed., CRC Press, Boca Raton, 2007, p 31–47
3. M.-H. Tsai, High-Entropy Alloys: A Critical Review, *Mater. Res. Lett.*, 2014, **2**(3), p 107–123
4. Y. Zhang, Solid-Solution Phase Formation Rules for Multi-Component Alloys, *Adv. Eng. Mater.*, 2008, **10**(6), p 534–538
5. W.R. Wang, Phases, Microstructure and Mechanical Properties of $\text{Al}_x\text{CoCrFeNi}$ High-Entropy Alloys at Elevated Temperatures, *J. Alloys Compd.*, 2014, **589**, p 143–152
6. W.R. Wang, Effects of Al Addition on the Microstructure and Mechanical Property of $\text{Al}_x\text{CoCrFeNi}$ High-Entropy Alloys, *Intermetallics*, 2012, **26**, p 44–51
7. J. Joseph, Understanding the Mechanical Behaviour and the Large Strength/Ductility Differences Between FCC and BCC $\text{Al}_x\text{CoCrFeNi}$ High Entropy Alloys, *J. Alloys Compd.*, 2017, **726**, p 885–895
8. H.P. Chou, Microstructure, Thermophysical and Electrical Properties in $\text{Al}_x\text{CoCrFeNi}$ ($0 \leq x \leq 2$) High-Entropy Alloys, *Mater. Sci. Eng. B*, 2009, **163**(3), p 184–189
9. M. Komarasamy, Effect of Microstructure on the Deformation Mechanism of Friction Stir-Processed $\text{Al}_{0.1}\text{CoCrFeNi}$ High Entropy Alloy, *Mater. Res. Lett.*, 2015, **3**(1), p 30–34
10. N. Kumar, High Strain-Rate Compressive Deformation Behavior of the $\text{Al}_{0.1}\text{CrFeCoNi}$ High Entropy Alloy, *Mater. Des.*, 2015, **86**, p 598–602
11. F. Otto, The Influences of Temperature and Microstructure on the Tensile Properties of a CoCrFeMnNi High-Entropy Alloy, *Acta Mater.*, 2013, **61**(15), p 5743–5755
12. A. Gali, Tensile Properties of High- and Medium-Entropy Alloys, *Intermetallics*, 2013, **39**, p 74–78
13. S. Asgari, Strain Hardening Regimes and Microstructural Evolution During Large Strain Compression of Low Stacking Fault Energy FCC Alloys that Form Deformation Twins, *Metall. Mater. Trans. A*, 1997, **28**(9), p 1781–1795
14. Y.Z. Tian, Significant Contribution of Stacking Faults to the Strain Hardening Behavior of Cu-15% Al Alloy with Different Grain Sizes, *Sci. Rep.*, 2015, **5**, p 16707
15. G.K. Williamson, X-Ray Line Broadening from Filed Aluminium and Wolfram, *Acta Metall.*, 1953, **1**(1), p 22–31
16. G.K. Williamson, III. Dislocation Densities in Some Annealed and Cold-Worked Metals from Measurements on the X-Ray Debye-Scherrer Spectrum, *Philos. Mag.*, 1956, **1**(1), p 34–46
17. M. Karolus, Crystallite Size and Lattice Strain in Nanocrystalline Ni-Mo Alloys Studied by Rietveld Refinement, *J. Alloys Compd.*, 2004, **367**(1-2), p 235–238
18. S. Kumari, Strain Anisotropy in Freestanding Germanium Nanoparticles Synthesized by Ball Milling, *J. Nanosci. Nanotechnol.*, 2009, **9**(9), p 5231–5236
19. M. Komarasamy, Serration Behavior and Negative Strain Rate Sensitivity of $\text{Al}_{0.1}\text{CoCrFeNi}$ High Entropy Alloy, *Intermetallics*, 2017, **84**, p 20–24
20. X. San, Effect of Stacking Fault Energy on Mechanical Properties of Ultrafine-Grain Cu and Cu-Al Alloy Processed by Cold-Rolling, *Trans. Nonferr. Met. Soc. China*, 2012, **22**(4), p 819–824
21. S.W. Wu, Strong Grain-Size Effect on Deformation Twinning of an $\text{Al}_{0.1}\text{CoCrFeNi}$ High-Entropy Alloy, *Mater. Res. Lett.*, 2017, **5**(4), p 276–283
22. X.D. Xu, Transmission Electron Microscopy Characterization of Dislocation Structure in a Face-Centered Cubic High-Entropy Alloy $\text{Al}_{0.1}\text{CoCrFeNi}$, *Acta Mater.*, 2018, **144**, p 107–115
23. T.H. Courtney, *Mechanical Behavior of Materials*, Waveland Press, Long Grove, 2005